Available online at www.sciencedirect.com

SciVerse ScienceDirect

Solar Energy 87 (2013) 76–83

SOLAR ENERGY

www.elsevier.com/locate/solener

Heating season performance of a full-scale heat pipe assisted solar wall

Brian S. Robinson, Nicholas E. Chmielewski, Andrea Knox-Kelecy, Ellen G. Brehob, M. Keith Sharp *

Renewable Energy Applications Laboratory, Department of Mechanical Engineering, University of Louisville, 200 Sackett Hall, Louisville, KY 40292, United States

Received 7 March 2012; received in revised form 28 September 2012; accepted 12 October 2012
Available online 16 November 2012

Communicated by: Associate Editor H.-M. Henning

Abstract

Previous computer simulations and bench-scale experiments showed that the heat pipe assisted solar wall had the potential for significantly improved performance relative to conventional passive space heating systems. To further test this potential, a full-scale prototype of the heat pipe system was designed, built and installed in a classroom on the University of Louisville campus in Louisville, KY. During the spring heating season of 2010 (January–April), maximum daily peak thermal efficiency was 83.7% and average daily peak thermal efficiency was 61.4%. The maximum hourly average room gain achieved during the season was 163 W/m^2. On days with good solar insolation, the thermal storage was heated to temperatures sufficient to provide significant energy to the classroom – even during the coldest days of the season. During the longest period (4 days) of low insolation during the season, average hourly heat delivery to the room from storage remained positive, and was never less than 16.6 W/m^2. During good insolation days following a period of consecutive low insolation days, thermal storage temperature was quickly restored to levels comparable to those obtained during consecutive good insolation days. Estimated heat removal factor $*$ transmittance absorptance product $F_R(\tau\alpha)$ and heat removal factor $*$ overall loss coefficient $F_R U_L$ values for the system were comparable to those for glazed liquid active collectors.

Keywords: Solar; Passive; Heat pipe; Space heating; Water wall; Isolated gain

1. The heat pipe augmented solar space heating system

1.1. System fundamentals

The heat pipe augmented solar space heating system (Corliss, 1979; Susheela and Sharp, 2001) is a type of isolated gain passive heating system. Isolated gain systems experience solar gains via a collector system that does not cause increased losses through the south wall of the building, as glass windows do in direct and indirect gain systems. This "thermal diode" effect significantly improves system performance. Conventional systems (Fig. 1) require a substantial elevation difference between the collector and storage/room to drive thermosyphoning of a single-phase fluid. However, two-phase heat transfer in a heat pipe allows the system to operate with a small elevation difference so that the entire system can be installed in the south wall (Fig. 2).

When insolation on the absorber raises the temperature of the evaporator section above that of the condenser section, the liquid inside is boiled into a vapor (Fig. 3). The vapor then rises through the adiabatic section, which passes through the insulated wall of the building, and reaches the condenser end where the vapor condenses and transfers its energy to the thermal mass. The condensed liquid then flows back to the evaporator section by gravity, completing the cycle.

* Corresponding author. Tel.: +1 502 852 7280; fax: +1 502 852 6053.
E-mail address: keith.sharp@louisville.edu (M.K. Sharp).

0038-092X/$ - see front matter © 2012 Elsevier Ltd. All rights reserved.
http://dx.doi.org/10.1016/j.solener.2012.10.008

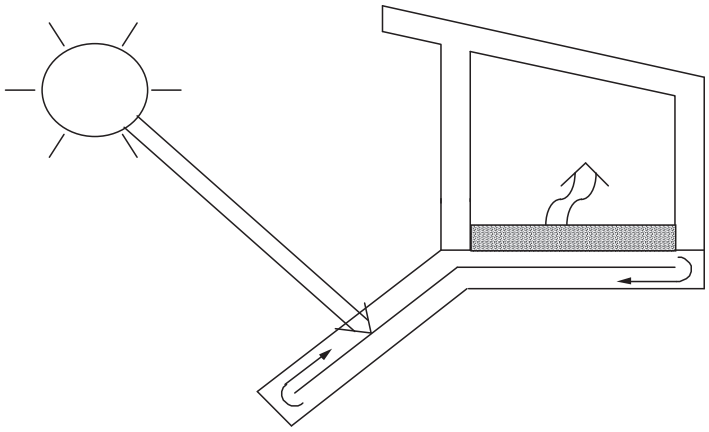

Fig. 1. Isolated gain passive solar system with thermosyphoning collector.

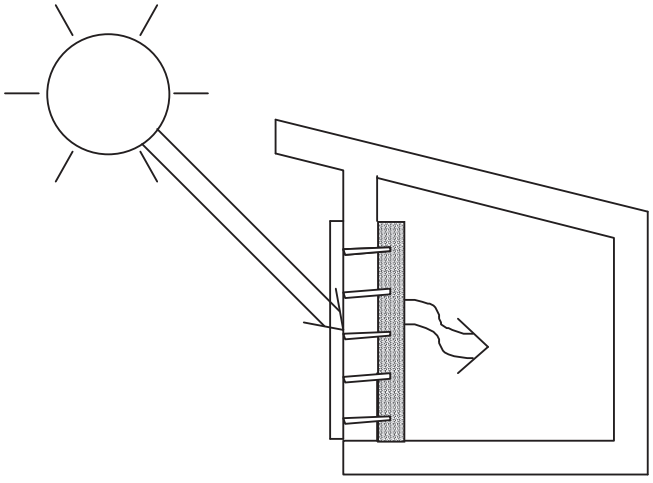

Fig. 2. Isolated gain passive solar heating system with five heat pipes between the absorber and thermal mass.

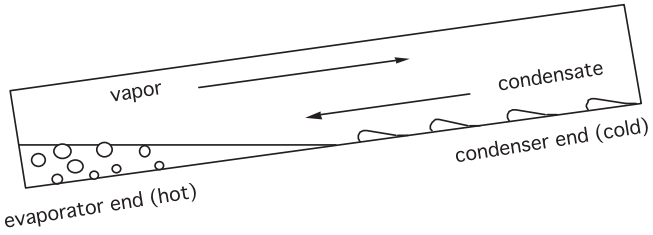

Fig. 3. Schematic of heat pipe operation.

1.2. Previous work

Susheela and Sharp (2001) designed and tested a heat pipe system that could be installed on existing homes without demolishing the wall of the building. The absorber portion was mounted on the outside of a south-facing wall, with water contained in tanks as the thermal mass on the inside of the wall. Holes were drilled in the existing wall for the adiabatic sections of the heat pipes to pass through, connecting the absorber and water tanks. The heat pipes had a 5° slope throughout and were made from copper pipe with 1 in. inner diameter, with DuPont SUVA-124 refrigerant (chlorotetrafluoroethane) as the working fluid and a stainless steel wire wicking structure. Experiments were performed outdoors, and system efficiencies (defined as the ratio of power delivered to the room over incident insolation) reached as high as 60% during sunny days. Computer simulations were also performed to model the performance of the unit.

Albanese et al. (2012) followed Susheela and Sharp's recommendations for improvements on their design, and developed computer simulations for similar heat pipe systems. Computer simulations were run for a large number of variations in system parameters, including glazing characteristics, selective surfaces, absorber thicknesses, insulation properties, and the number and material of heat pipes. Parametric studies showed that several parameters had minimal effect on system performance relative to the baseline design, including number of covers, absorber thickness and material, collector edge insulation, heat pipe material, number of heat pipes, tank wall conductivity and thickness, tank to room conductance, condenser fins, and wall insulation. Therefore, compromises in these areas to reduce system cost while maintaining good thermal performance are possible. Parameters with greater effect on system performance were cover thickness and extinction coefficient, absorber surface properties and thermal storage capacity; with a thin low-iron glass cover, a high-performance selective absorber surface and large storage capacity being favorable.

Additionally, Albanese et al. (2012) constructed a bench-scale experimental model to further assess parametric heat pipe system performance. A fill level of 120% of the evaporator volume produced the highest system efficiency, and insulating the adiabatic section of the heat pipe improved efficiency for all fill levels. The addition of condenser fins did not significantly improve system performance. Utilizing the optimal parameter values, a system efficiency of 85% was attained.

To better understand system performance in realistic weather conditions, in particular, the relatively cloudy

and cool conditions in Louisville, KY, a full-scale experimental prototype was constructed and installed in a classroom on campus, facing 10° east of south. This paper will outline prototype design and construction, and report prototype performance for the spring 2010 heating season in Louisville.

2. Methods

2.1. Prototype design and construction

The design (Fig. 4) consisted of five individual heating units, each with an absorber plate, heat pipe and water tank (Chmielewski, 2009). The evaporator section was glued and clamped to an aluminum absorber. The adiabatic section of the heat pipe extended through a layer of thermal insulation to the condenser, which was placed within a water tank for thermal mass. An aluminum frame supported and enclosed the five sets of absorbers, heat pipes, and water tanks, as well as a glazing on the south side of the assembly. The north side of the system was faced with a screen that allowed free convection and radiation from the thermal mass to the room.

The 1.588 mm thick frame was 2.09 m tall × 1.25 m wide × 0.394 m deep and was constructed with a 0.0191 m wide mounting flange to seal around the glass glazing on the south side of the system. The 2.06 m (81 in.) × 1.22 m (48 in.) glazing consisted of 3.18 mm (1/8 in.) thick low-iron glass with an anti-reflective coating. The glazing edges were protected with a silicone rubber extrusion and were clamped into place using a front mounting flange along the outer edge of the frame.

The absorber plates of the unit consisted of 3.18 mm thick aluminum plated with black chrome over a nickel substrate. Semi-circular grooves were formed in the absorber plates to receive the heat pipes. The outside edges of the absorber plates were mounted to the support frame with aluminum screws with insulating plastic spacers. The gap between the absorber plates and the glazing was 0.0254 m. The total receiving face of the absorber plates was 2.02 m (79½ in.) tall × 1.194 m (47 in.) wide.

The heat pipes were constructed from 0.0254 m (1 in.) inner diameter and 0.0286 m outer diameter copper pipes. The lengths of the evaporator, adiabatic and condenser sections were 1.16 m (45½ in.), 0.229 m (9 in.), and a 1.09 m (43 in.), respectively. All sections of the heat pipe were mounted at 5° from the horizontal. A 6.35 mm diameter fitting for filling the heat pipes was formed in the adiabatic section.

Filling of the heat pipes was achieved using a charging system consisting of a vacuum pump, refrigerant tank, vacuum gauge, and several control valves. The entire charging system was drawn to a vacuum of 86.4 kPa (648 mmHg) with the vacuum pump. Each heat pipe was filled with

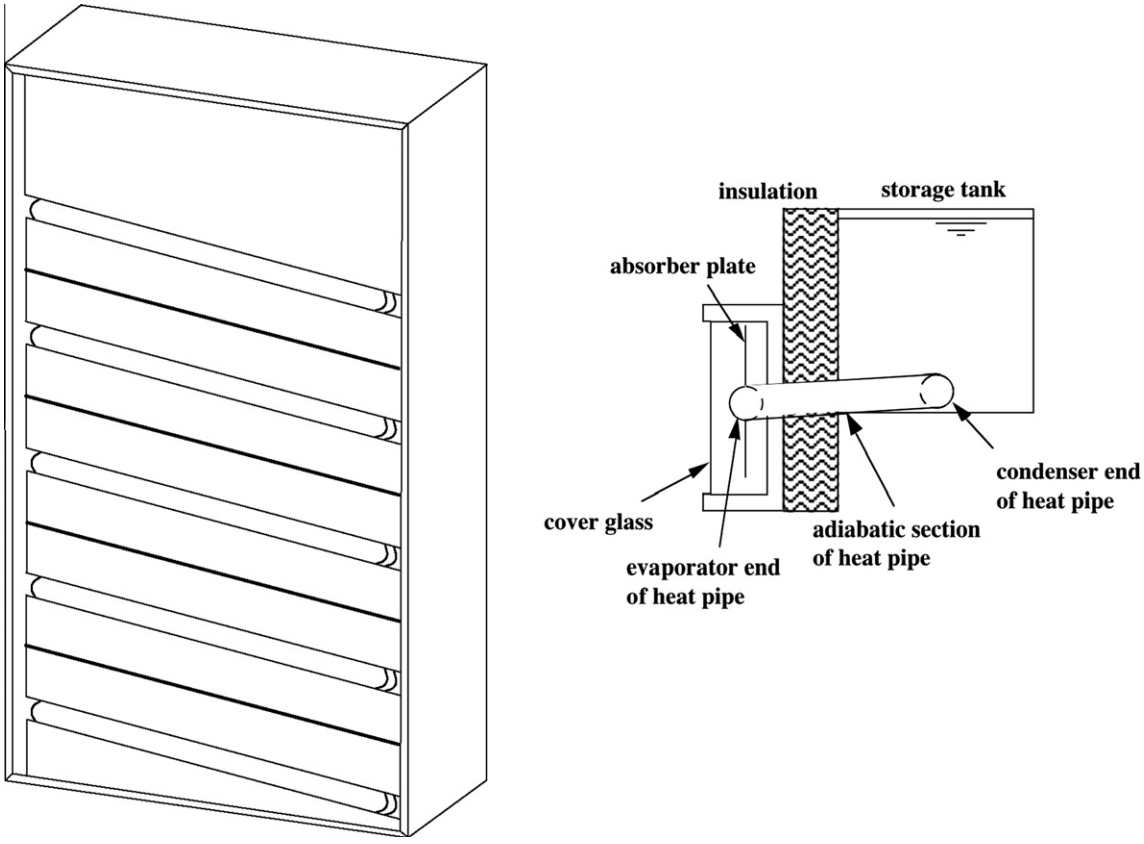

Fig. 4. Left: isometric sketch of the prototype. On the front are the five slanted evaporator sections and absorber plates as seen through the cover glass. The interior components are not visible. Right: 2D schematic of one unit.

957 g of DuPont SUVA-124. This amount corresponded to a liquid volume of 120% of the evaporator section, as recommended by Albanese et al. (2012).

The heat pipes were glued into the grooves in the absorber plates with high thermal conductivity epoxy. In addition, 3.18 mm thick aluminum clamps 1.09 m long × 0.102 m wide held the heat pipes in place while the glue set, and were left in place.

Plastic tanks 1.11 m long × 0.356 m tall × 0.203 m thick (43½ in. × 14 in. × 8 in.) contained water as thermal mass. A threaded bulkhead fitting on the end of the tank near the bottom allowed for the heat pipe entrance. Water capacity was 65.1 l per tank. Total weight of the system was 487 kg, consisting of 326 kg of water and an installation or "dry" weight of 161 kg.

Insulation of the unit included 0.0508 m of mineral wool (RSI-1.41 K m^2/W, (R-8.0 h ft^2 °F/Btu)) next to the absorber plates to prevent outgassing in case of overheating, three layers of 0.0217 m Styrofoam (RSI-0.528 K m^2/W (R-3.0 h ft^2 °F/Btu) per panel), and 0.0254 m thick mineral wool pipe wrap was used around the adiabatic section of the heat pipes.

2.2. Instrumentation

Eight T-type thermocouples were placed in the center water tank, four each at two different depths, to assess stratification as well as temperature variations in the horizontal direction. Single thermocouples were placed in each of the other tanks. An additional thermocouple was placed in the room to measure room temperature. Two Kipp & Zonen CM3 solar pyranometers were used to measure insolation values, with one centered directly above the unit and the second directly below the unit. All data was collected using a National Instruments SCXI platform in conjunction with a low-voltage thermocouple-designed SCXI-1102/B/C module. A SCXI-1600 analog to digital converter was used for the analog data inputs. LabVIEW software was used to sample and log the data at a sampling rate of 0.01667 Hz (one sample each minute). Hourly ambient temperature data was obtained from nearby Bernheim Arboretum and Research Forest.

2.3. Data analysis

Data was collected and analyzed for January through April of 2010. Thermal efficiency of the system, η, was calculated by

$$\eta = \frac{\dot{Q}_{in}}{SA_c} \tag{1}$$

where $\dot{Q}_{in}$ represents the useful gain transferred to the thermal mass by the heat pipe, S is the insolation received by the collector and A_c is the collector area. Days for which the hourly average radiation was less than 100 W/m^2 included hours in which $\dot{Q}_{in}$ was negative, signifying rainy or very cloudy conditions, and were discarded from the analysis. All hourly values of $\dot{Q}_{in}$ were positive during every day in which the hourly average radiation was greater than 100 W/m^2.

An existing overhang caused shading on the prototype when the solar zenith angle, θ_z, was less than 48.2°, which occurred from February to October. When the system was shaded, insolation on the system was estimated by

$$S = xS_{diffuse} + (1-x)S_{total} \tag{2}$$

where x is the fraction of shading, and $S_{diffuse}$ was measured by the shaded upper pyranometer and S_{total} was measured by the unshaded lower pyranometer. The fraction of shading is given by

$$x = \frac{\frac{a}{\tan\theta_z} - b}{h} \tag{3}$$

where the horizontal overhang distance $a = 0.711$ m (28 in.), the vertical distance between the aperture and the overhang b = 0.768 m (30.25 in.), the perture height $h = 2.02$ m (79.5 in.) and the solar zenith angle is

$$\theta_z = \cos^{-1}[\cos\phi\cos\delta\cos\omega + \sin\phi\sin\delta] \tag{4}$$

where the latitude is $\phi = 38.3°$, δ is the declination and ω is the hour angle. The shading fraction during the period of analysis ranged from 0 to 0.75.

To determine $\dot{Q}_{in}$, conservation of energy applied to the tank gives

$$\dot{Q}_{in} = \dot{Q}_{st} + \dot{Q}_{out} \tag{5}$$

where $\dot{Q}_{st}$ represents the rate of increase of energy in the thermal mass and $\dot{Q}_{out}$ is the rate of energy transfer from the tank to the room. $\dot{Q}_{st}$ is

$$\dot{Q}_{st} = \frac{m_{H_2O}c_{p,H_2O}\Delta T_{H_2O}}{\Delta t} \tag{6}$$

where m_{H_2O} is the mass of the water used for thermal storage, c_{p,H_2O} is the specific heat of the water, and ΔT_{H_2O} is the water temperature change during time interval Δt, which was one hour. $\dot{Q}_{out}$ is

$$\dot{Q}_{out} = \frac{T_{H_2O,avg} - T_{room,avg}}{R_{total}} \tag{7}$$

where $T_{H_2O,avg}$ and $T_{room,avg}$ are the average temperature during the hour for the water and room, respectively, and R_{total} is the total thermal resistance from the thermal mass to the room air. Temperature in the room could not be controlled in these experiments, and varied according to the use of the room for classes and thermostat setbacks when the room was not in use. A thermal resistance network for R_{total} is shown in Fig. 5.

The network included convection on the inside surface of the tank wall, $R_{H_2O,conv}$, conduction through the tank wall, R_{cond}, and parallel radiation, R_{rad}, and convection, $R_{air,conv}$, from the wall of the tank to the room. Applying the resistance network shown in Fig. 5, R_{total} is

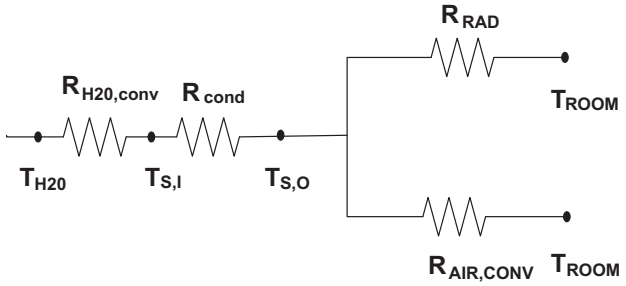

Fig. 5. Thermal resistance network from the thermal mass to the room.

$$R_{total} = R_{H^2O,conv} + R_{cond} + \left(\frac{1}{R_{rad}} + \frac{1}{R_{air,conv}}\right)^{-1} \quad (8)$$

$R_{H_2O,conv}$ and $R_{air,conv}$, respectively, are

$$R_{H_2O/air,conv} = \frac{1}{h_{H_2O/air,conv} A_t} \quad (9)$$

where A_t is the cross-sectional area of the tank wall and the convection coefficient for water or air is

$$h_{H_2O/air,conv} = \frac{k_{H_2O/air} Nu_{H_2O/air}}{L} \quad (10)$$

where $k_{H_2O/air}$ is the thermal conductivity for water or air, L is the tank wall height, and the Nusselt number, $Nu_{H_2O/air}$ (developed for free convection from a vertical plate (Incropera and DeWitt, 2007)), for water or air is dependent on whether tank conditions are laminar or turbulent. Transition depended on the Rayleigh number

$$Ra_{H_2O/air} = \frac{g\beta_{H_2O/air}\Delta T_{H_2O/air} L^3}{v_{H_2O/air}\alpha_{H_2O/air}} \quad (11)$$

where g is the gravitational constant of acceleration, β is the volumetric thermal expansion coefficient, v is kinematic viscosity and α is thermal diffusivity for water or air, and the temperature difference between mediums is

$$\Delta T_{H_2O} = T_{\infty,H_2O} - T_s \quad (12)$$

or

$$\Delta T_{air} = T_s - T_{\infty,air} \quad (13)$$

where T_{∞,H_2O} was approximated as the tank water temperature, $T_{\infty,air}$ was approximated as the room temperature, and the tank surface temperature, T_s, was approximated as the average temperature between the tank water and room air. For $Ra_{H_2O/air} < 10^9$ (laminar), the Nusselt number is

$$Nu_{H_2O/air} = 0.68 + \frac{0.67(Ra_{H_2O/air})^{1/4}}{(1 + (0.492/\mathrm{Pr}_{H_2O/air})^{9/16})^{4/9}} \quad (14)$$

where $Pr_{H_2O/air}$ is the Prandtl number. When $Ra_{H_2O/air} < 10^9$ (turbulent), the Nusselt number is

$$Nu_{H_2O/air} = \left[0.825 + \frac{0.387(Ra_{H_2O/air})^{1/6}}{(1 + (0.492/\mathrm{Pr}_{H_2O/air})^{9/16})^{8/27}}\right]^2 \quad (15)$$

where the conductive resistance through the tank wall is

$$R_{cond} = \frac{th}{k_{wall} A_c} \quad (16)$$

where th is the tank wall thickness and k_{wall} is the thermal conductivity of the tank wall. Finally, the radiative resistance is

$$R_{rad} = \frac{1}{h_{rad} A_c} \quad (17)$$

where

$$h_{rad} = \varepsilon\sigma(T_s + T_{\infty,air})(T_s^2 + T_{\infty,air}^2) \quad (18)$$

where ε is the radiative emissivity of the water tank wall and σ is the Stefan–Boltzmann constant.

The thermophysical properties of the water in the tank and the air in the room were determined by interpolation from thermophysical property tables (Incropera and DeWitt, 2007) at the average temperatures over the course of that hour. The volumetric thermal expansion coefficient β was also interpolated in the same manner for water, while β for air, assumed to be an ideal gas, was calculated using

$$\beta = \frac{1}{T_{room,avg}} \quad (19)$$

Thermal diffusivity is

$$\alpha = \frac{k}{\rho c_{p,H_2O/air}} \quad (20)$$

where $c_{p,H_2O/air}$ is the specific heat of the applicable medium $c_{p,H_2O} = 4186$ J/(kg K) and $c_{p,air} = 1005$ J/(kg K). Kinematic viscosity is

$$v = \frac{\mu}{\rho} \quad (21)$$

The mass of the water in each tank is

$$m_{water} = \rho V_{tnk} \quad (22)$$

where V_{tnk} is the volume of each tank.

Energy gain rates were calculated for each heating unit, and summed to obtain total system gains to calculate system efficiency. To estimate the characteristic performance of the system for clear sky radiation normal to the aperture, a time constant for the collector was estimated by applying exponential curve fits to the decay in absorber temperature after sundown ($S \leqslant 0$ W/m^2). Only nights with ambient temperature variation less than ± 1.5 °C (from ASHRAE standard 93 [2010] for testing active solar collectors) and coefficient of determination $R^2 > 0.96$ were included.

Efficiency versus loss potential to insolation ratio $(T_s - T_a)/S$ was also calculated. Note that this ratio is similar to that used to determine a performance curve for an active solar collector $(T_i - T_a)/S$, where T_i is the inlet temperature to the active collector. Thermal storage temperature T_s is a close analog of inlet temperature to the absorber in this passive system. Conditions for these effi-

ciency estimates were selected to conform as closely as possible to ASHRAE standard 93 [2010], including variations in isolation less than ±32 W/m^2 for intervals of 10 min or two collector time constants, which ever is greater.

2.4. Error propagation

The thermocouples had an uncertainty of ±0.1 K and the pyranometers had an overall error of ±2% (±18.4 W/m^2), as specified by the manufacturer Kipp and Zonnen. Upon calibration the absolute accuracy of the SCXI-1600 and SCXI-1102 modules was ±2.4 mV and ±0.25 K, resulting in overall uncertainty in temperature measurement of 0.27 K. The estimated uncertainty in the calculated system efficiency was therefore 0.72%.

3. Results

Hourly average insolation on the system SA_c, room gain $\dot{Q}_{out}$, tank temperature, room temperature and ambient temperature are shown for two conditions in Figs. 6 and 7 to illustrate the range of system response. First, system response is shown for consecutive days (January 28 and 29) with high and low insolation, respectively, in Fig. 6. January 28 (Julian hours 649–672) represented the best insolation during the heating season. The following day (Julian hours 673–696) had little insolation and was also the coldest day of the heating season. Tank temperature rose sharply to as high as 24 K (43 °F) above the room temperature on January 28, however on January 29, the gradual decline in tank temperature was continuous throughout the day, dropping to about 10 K (18 °F) above room temperature. The room gain followed this trend.

Second, the same hourly average powers and temperatures are shown for a series of five consecutive days with low insolation in Fig. 7. These days followed four consecutive days of good insolation, thus the difference between tank and room temperatures began on the first day (February 22, Julian hours 1249–1272) at 13 K (23 °F). The gradual decline in this temperature difference is only slightly interrupted on February 22 and 23 (Julian hours 1273–1296), two days with very low insolation. For the following two days with low insolation, February 24 (Julian hours 1297–1320) and 25 (Julian hours 1321–1344), small gains occur sufficient to maintain the temperature difference above 5 K (9 °F). On February 26 (Julian hours 1345–1368), with peak hourly insolation on the unit exceeding 830 W/m^2, the temperature difference was restored to 17 K (31 °F). Heat transfer to the room remains positive throughout this period, never dropping below 40 W.

Hourly average useful gain $\dot{Q}_{in}$ versus hourly average solar input SA_c for hours from 9 am to 5 pm, are shown in Fig. 8.

Peak system efficiencies were calculated for each day. The maximum daily peak efficiency calculated was 83.7%, and the average daily peak efficiency calculated was 61.4%. The maximum daily peak efficiency was achieved on February 8, an unusually warm day with an average ambient temperature of 21.4 °C (70.6 °F) versus an average storage temperature of 20.6 °C (69.1 °F). (Thus for these conditions, the absorber gained energy not only from insolation, but also from ambient air, which raises the potential for efficiencies defined in terms of the insolation source

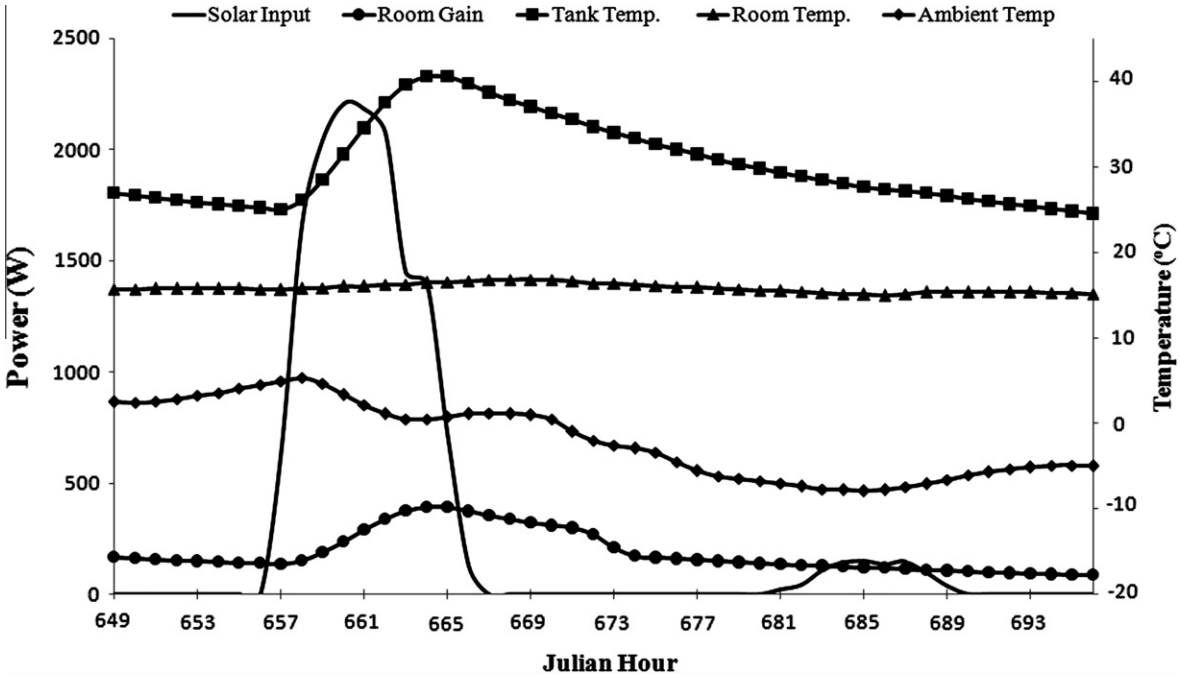

Fig. 6. Average hourly values for insolation, room gain, and tank, room and ambient temperatures for January 28 and 29.

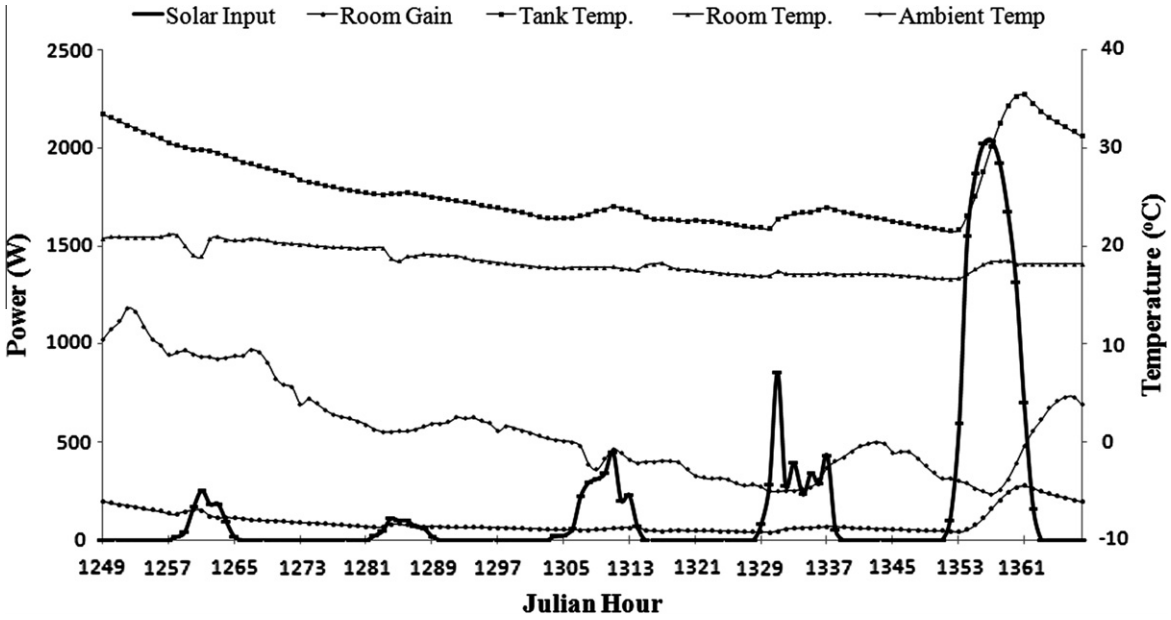

Fig. 7. Average hourly values for system trends for February 22–26.

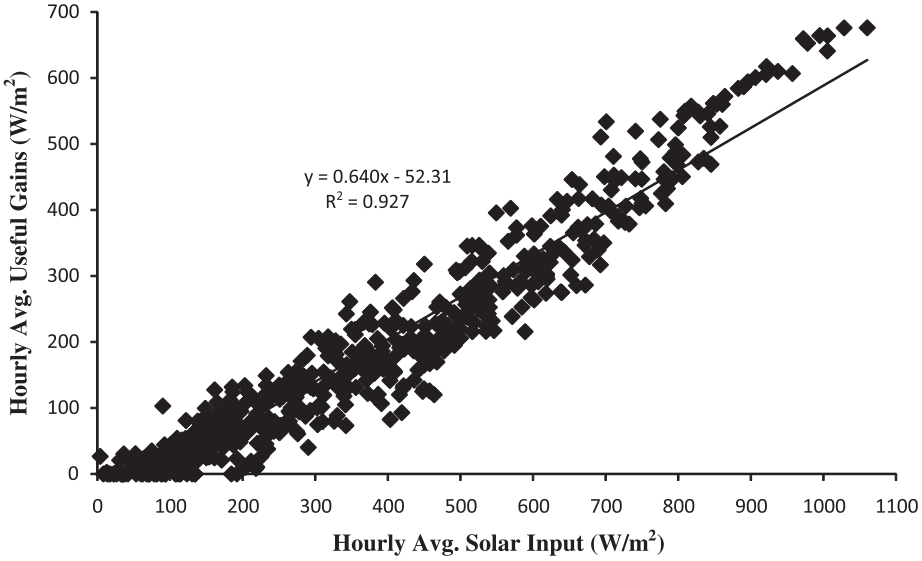

Fig. 8. Plot of hourly average useful gains versus hourly average solar input from 9 am to 5 pm for each day of the heating season.

only (Eq. (1)) to be greater than 100%. Such conditions also frequently occur during the summer for domestic water heating and pool heating systems.) This was the only day during the heating season in which average ambient temperature exceeded average storage temperature.

Collector efficiency is plotted in Fig. 9 versus the ratio of the temperature difference between storage and ambient over absorbed insolation. Because the collector is non-tracking, the ASHRAE 93 [2010] limit on insolation variation during two time constants (the collector time constant was calculated to be 90 min) could not be met. 50 min intervals met all other ASHRAE 93 criteria, and provided a reasonable number of samples for the plot. To meet the insolation variation limit, all samples were near solar noon. The curve fit implies a system efficiency of 74.1% when storage temperature equals ambient temperature. The angle of incidence of beam radiation on the system at solar noon varied from 31.7° (January 13) to 62.7° (April 18).

4. Discussion

Even though the average ambient temperature was a cold 2 °C (36 °F) on January 28, the tank temperature still reached a peak hourly value of 41 C (105 °F) (Fig. 6), which highlights the effectiveness of solar energy collection and heat transfer of the heat pipe system. Room gains, which are primarily driven by the temperature difference

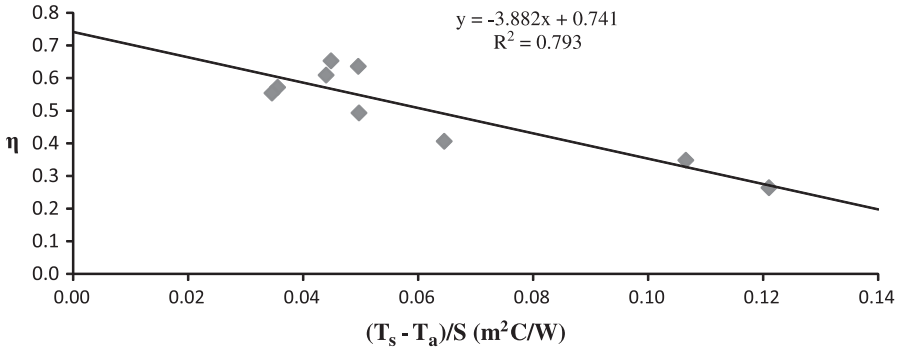

Fig. 9. System efficiency versus loss potential/insolation ratio.

between the tank and room, reached 163 W/m^2 – the highest hourly average value during the heating season.

The sequence of four cloudy days in Fig. 7 represents a near worst-case scenario for the period of data collection regarding available solar resource and system contributions to room heating. Yet for this sequence, small useful solar gains occurred, and room gain remained significant. Another sequence of three very cloudy days on February 27–March 1 (not shown) caused tank temperature to come even closer to room temperature, decreasing room gain to near zero. Larger thermal capacity could bridge longer spans of unfavorable weather, but would seldom be required and would increase system cost. This tradeoff is typical for utilization of an intermittent energy resource to meet an unpredictable load, and warrants scrutiny as a design parameter for a commercial product.

The trendline shown in Fig. 8 suggests that useful gains will occur when solar input exceeds a mean of 83 W/m^2. The slope of the trendline represents an asymptotic thermal efficiency of 64%, comparable to the calculated system average peak efficiency of 61.4%. While the coefficient of determination for the curve fit of this data is good, the threshold for utilizable insolation varies from zero to over 200 W/m^2. In addition, useful gain varies by a factor of two or more for low insolation. This wide range is explained in part by the omission in this graph of the dependence of useful gains on ambient and absorber temperatures.

Fig. 9 accounts for this temperature dependence in a way that is novel for passive solar systems, but is standard for active solar collectors. For a heat pipe, the temperature of the condensate entering the evaporator section is nearly equal to the storage temperature. Thus storage temperature represents an accessible analog of collector inlet temperature, which makes the parameter on the abscissa of Fig. 9 comparable to that used for active collectors. The intercept and slope of the trendline (0.741 and −3.88 W/m^2 K) are analogous to the heat removal factor $*$ transmittance absorptance product $F_R(\tau\alpha)$ and heat removal factor $*$ overall loss coefficient $F_R U_L$, respectively, for active collectors. These parameter values for the passive system compare favorably to average values for glazed liquid active collectors, which are $F_R(\tau\alpha) = 0.703$ and $F_R U_L = -4.74$ W/m^2 K (SRCC, 2012). The incidence angle modifier, another standard index of active collector performance, could not be determined for the passive system because data was not available for low angle of incidence.

The time constant for the passive collector is considerably longer than that for active collectors, which typically ranges from 1 to 15 min. Several factors may account for this, including the increased thermal capacity associated with additional collector material (3.18 mm thick aluminum absorbers plus the copper heat pipes), a higher specific heat for HCFC-124 than for water or antifreeze solutions, and additional enthalpy associated with latent heat of the phase change fluid.

Potential improvements to the experimental setup include testing in a facility where overhangs and shading can be eliminated, where the surface azimuth is perfectly south, and where room use and energy gains can be controlled. Improvements in system performance may also be possible with increased insulation between the thermal mass and the absorber, as well as by modifying the design of the frame to reduce losses to ambient and a less thermally-conductive material for the adiabatic section to eliminate losses from storage during cloudy and nighttime conditions.

References

Albanese, M.V., Robinson, B.S., Brehob, E.G., Sharp, M.K., 2012. Simulated and experimental performance of a heat pipe assisted solar wall. Solar Energy 86, 1552–1562.

Chmielewski, N.E., 2009. Design, construction, and experimentation of a heat pipe augmented solar wall. MS thesis, Department of Mechanical Engineering, University of Louisville.

Corliss, J.M., 1979. Evaluation of heat pipe application for passive solar systems. DOE report, September 1979.

Incropera, F.P., DeWitt, D.B., 2007. Introduction to Heat Transfer, 5th ed. Wiley, Hoboken, NJ.

SRCC, 2012. Solar Rating and Certification Corporation. <http://www.solar-rating.org/ratings/ og100.html>. (accessed 22. 01. 2012).

Susheela, N., Sharp, M.K., 2001. A heat pipe augmented passive solar system for heating of buildings. J. Energy Eng. 127 (1), 18–36.